Co-published by
Institute of Fluid-Flow Machinery
Polish Academy of Sciences
Committee on Thermodynamics and Combustion
Polish Academy of Sciences

http://www.imp.gda.pl/archives-of-thermodynamics/

Measurements of electrical capacitance in the flow of reservoir fluid with gas bubbles

Remigiusz Ornowski[a,b*], Stanisław Żwan[a]

[a]TERCJA Measuring and Computer Systems, Dywizjonu 303 5B/24, 80-462 Gdańsk, Poland
[b]Institute of Fluid Flow Machinery, Polish Academy of Sciences, ul. Fiszera 14, 80-231 Gdańsk, Poland
*Corresponding author email: rornowski@imp.gda.pl

Received: 18.08.2025; revised: 01.09.2025; accepted: 11.09.2025

Abstract

The paper discusses tests of an electric capacitance sensor designed and built to measure gas fraction in a reservoir fluid flow. These tests were conducted under conditions typical for oil field testing and productivity monitoring. In such an application, the electrical permittivity of the liquid and gas components is of the same order of magnitude, which poses a significant challenge in capacitance metering of the phase content. The studied two-electrode capacitance sensor is a novel design. It uses a commercial, high-resolution ΔΣ capacitance-to-digital converter. The sensor was experimentally tested on the flow of reservoir fluid (from Lubiatów-Międzychód-Grotów field in Poland) heated to 40–50°C to reproduce field conditions during actual gas and oil extraction. The gas fraction in the reservoir fluid was generated by the injection of air or methane bubbles. Fluid velocities during the testing ranged from 1 to 3.1 m/s, and the void fraction reached 4.4%. After calibration, the examined capacitance sensor was able to detect a void fraction as low as 1%. The measured capacitance differences due to gas content were dependent on the spatial distribution of voids in the inter-electrode space. This effect was confirmed by photographs of the flow patterns and numerical simulations of the electric field distributions.

Keywords: Capacitance sensor; Reservoir fluid; Oil-gas flow; Oil and gas extraction; ΔΣ capacitance-to-digital converter;

Vol. 46(2025), No. 3, 39–49; doi: 10.24425/ather.2025.154922

Cite this manuscript as: Ornowski, R., & Żwan, S. (2025). Measurements of electrical capacitance in the flow of reservoir fluid with gas bubbles. *Archives of Thermodynamics*, 46(3), 39−49.

1. Introduction

Electrical capacitance measurement has a wide range of applications, both in industry and laboratory practice. In particular, it enables the measurement of the void fraction, i.e. the gas content in a liquid. Measuring gas content, both quantitatively and qualitatively, is crucial in many technological processes. One of the most important potential applications is two-phase liquid-gas flows, which are common, for example, in the refrigeration industry [1,2]. Detecting the presence of liquid at the steam turbine inlets is equally important. In the drilling industry, void fraction measurement is used during the drilling process to determine the amount of drilling fluid flowing from the well. This is a crucial parameter for blowout prevention. Using void fraction measurement during oil field sampling provides additional information about separator performance, which positively affects the control of operating parameters and separator efficiency. In the later stages of the oil field development, void fraction measurements are important for determining the phase composition of the reservoir fluid during well testing and productivity monitoring.

The most common method for measuring the phase composition of the reservoir fluid involves using a separator to measure each phase separately. This method is expensive and requires ongoing maintenance by qualified personnel. Due to the

Nomenclature

C – capacitance, F
E – electric field vector, V/m
n – unit normal vector
S – surface area, m^2
U – electric potential, V
V – voltage, V

Greek symbols
ε – absolute permittivity, F/m
ε_r – relative permittivity, –
ε_0 – vacuum permittivity, $\varepsilon_0 = 8.8541878188(14)\times10^{-12}$ F/m
φ – void fraction, –

Abbreviations and Acronyms
CDC – capacitance-to-digital converter
LMG – Lubiatów-Międzychód-Grotów

separator size, it also requires considerable space, which can be problematic on offshore drilling platforms. Due to the high inertia of the separator, this method has low time resolution but offers high measurement accuracy for quasi-steady flows. Therefore, implementing a system that allows for direct and continuous measurement of the void fraction without prior separation offers many advantages [3]. In this context, non-invasive and continuous capacitance measurement can be applied [4,5].

Over the years, many capacitance sensor designs based on analogue electronic circuits have been described in the literature. Salehi et al. [6], for instance, investigated a capacitance sensor aimed at measurements in oil–gas two-phase flow. The focus was on finding the optimal exciting frequency of the voltage applied to the electrodes. Based on the sensor impedance modelling and static experiments representing annular flow (with a void in the core) were made. They found that a frequency of 0.8–1.0 MHz gives the best sensitivity for the oil-gas medium. Continuing their research, Salehi et al. [7] investigated the performance of different electrode configurations for oil–gas flows in bubbly, plug, stratified and slug regimes. They concluded that an interlocking electrode arrangement (termed TRFLC) or a concave shape is best for identifying flow regimes. For measuring gas fraction, a helical shape is preferable. Ahmed and Ismail [8] also reviewed the performance of capacitance sensors with different electrode shapes.

In addition to previous studies, a system with a capacitance sensor specifically designed to measure water content in crude oil was constructed by Aslam and Tang [9]. Its electronics operated based on capacitance to phase angle conversion [10,11] and achieved a resolution of ±50 ppm of water content during laboratory tests on crude oil samples. A new design of the capacitance sensor also dedicated to oil-water flows was proposed by Demori et al. [12]. It was tested on an experimental setup with controlled two-phase annular and slug flows in a horizontal tube for oil fractions ranging from 20% to 65%.

Similarly, capacitance sensors with two concave, two helical, or double ring electrodes were experimentally investigated by dos Reis and da Silva Cunha [13] in water–air horizontal flow. Their study covered the full range of void fractions, from 0% to 100%. Their measurements showed that the highest sensitivity was observed for the concave electrodes, while the lowest for the double ring ones. However, measurements with concave electrodes were most dependent on the air–water flow patterns, and the double ring was least affected in this respect. The characteristics of the helical electrodes were similar to those of the double ring.

The problem of calibration of capacitance sensor was studied, among others, by Abou-Arkoub et al. [14]. They postulated that simple capacitance-sensing techniques can be used for online validation of multiphase flow meters. It was demonstrated that capacitance measurement combined with statistical and fuzzy-logic-type methods can provide the basis for a simple and robust validation of multiphase flow meters' performance by identifying the carrier, dispersed phase and flow structures. Furthermore, the proposed system could be retrofitted to existing multiphase flow meters.

Recent research has explored the use of digital signal processing in capacitance sensor electronics. For example, Wu et al. [15] used digital control in their combined conductance and capacitance sensor designed to measure water holdup in oil–water flow. Maurya and Parasuraman [16] built two- and four-electrode sensors for micro-droplet detection, which were based on the AD7150 capacitance-to-digital converter and were intended for use in drug delivery systems. Their sensor was mounted on an 8 mm outer diameter tube. It had a high sensitivity of 0.7409 fF/μL with repeatability of ±0.032%. Dos Santos et al. [5] developed an oil and gas pipeline monitoring system with a fast capacitance sensor designed for operation in hazardous areas. The sensor operated based on a resonant circuit with a 40 MHz reference oscillator with a frequency tolerance of ±100 ppm/K. The frequency output was digitised with a 15-bit resolution. Data was transmitted in real time to a microcomputer for analysis. The system achieved absolute uncertainty for a gas fraction content of 1.41% in slug flow.

The research presented below aimed to experimentally verify a two-electrode capacitance sensor using a commercially available high-resolution ΔΣ capacitance-to-digital converter (CDC).

The examined system is intended to be developed for use in real-time reservoir fluid characterisation, supporting well testing and productivity monitoring in the oil (petroleum) and gas industry. In this application, the electrical permittivity of liquid and gas components can be of the same order of magnitude, which constitutes a significant difficulty in capacitance metering of the phase content. Despite this, laboratory tests clearly demonstrate that the ΔΣ CDC enables the accurate detection of even small amounts of gas in reservoir fluid, successfully overcoming this difficulty. This finding highlights the capability and sensitivity of the system. Moreover, the measurements were carried out using the fluid at a temperature of 40–55°C, which is typical for oil and gas field production.

2. Materials and methods

The electrical capacitance in the pipe flow of reservoir fluid with gas bubbles was investigated experimentally using a capacitance

sensor of our design and construction. The measurements were made on a custom-built laboratory test stand with a horizontal test section.

2.1. Experimental setup

The test stand used during the present research is schematically shown in Fig. 1.

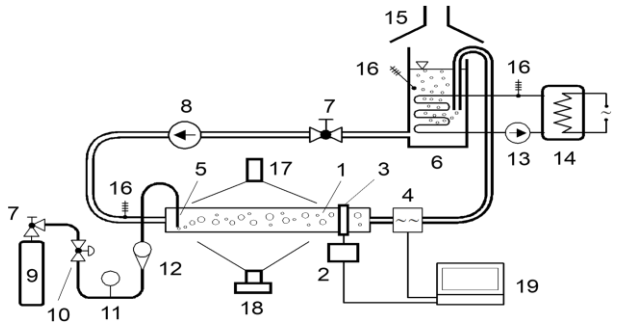

Fig. 1. Experimental setup: 1 – test section, 2 – capacitance sensor, 3 – measuring electrodes, 4 – ultrasonic flow meter, 5 – gas injection, 6 – degasser (flash tank), 7 – cut-off valve, 8 – reservoir fluid circulation pump, 9 – compressed gas cylinder (air or methane), 10 – gas flow control valve, 11 – gas pressure gauge, 12 – rotameter, 13 – heating water circulation pump, 14 – water heater, 15 – gas extraction chimney, 16 – temperature sensor, 17 – electronic flash, 18 – digital still camera, 19 – data acquisition.

It essentially consists of a loop in which the reservoir fluid circulates, including the test section 1 made of a horizontal, transparent polycarbonate tube with an internal diameter of 45 mm and a length of 400 mm. The electrodes 3 of the capacitance sensor 2 were precisely wrapped around the outer surface of this tube at a position near the downstream end. Upstream, a clean segment was used to observe and photograph gas bubbles injected by the needle 5, which was mounted at the beginning of the test section. Downstream of the test section, a polyamide tube segment served as the mounting point for the ultrasonic flow meter 4, with the instrument secured directly onto this segment. The rest of the loop was made of a rubber hose with an internal diameter of 50 mm. Between the flow meter and the circulating pump was the degasser 6, an open tank with a coil used for heating the fluid to the required temperature. The heating medium was water, which circulated between the degasser 6 and the electric boiler 14 via the pump 13. Gases (especially methane) separated from the reservoir fluid were removed from the laboratory through the extraction chimney 15. Downstream of the degasser tank 6, the cut-off valve 7 was installed. It was closed when the circulation pump 8 was turned off. Gas injected into the reservoir fluid was drawn from cylinder 9. The valve 10 adjusted its pressure to achieve the required flow rate. These parameters were monitored using the manometer 11 and the rotameter 12. To control the temperature, sensors 16 were placed at three specific locations: upstream of the test section, within the degasser and in the heating water loop. The flow pattern upstream of the capacitance sensor was photographed using the still camera 18, which was synchronised with the electronic flash 17. The readings from the capacitance sensor 2 and the ultrasonic flow meter 4, both fixed at their described positions, were recorded on-line and processed by laptop computer 19.

Main pump 8 of the centrifugal type was driven by a 2.2 kW electric motor. While the normal rotating speed of this pump was 1450 rpm, it was reduced by an inverter to achieve the required flow rate of the reservoir fluid. To determine this value, the flow velocity was measured with a Flexim Flexus F608 portable ultrasonic meter with an accuracy of ±0.005 m/s. The rotameter 12 (Brooks Instruments Sho-Rate glass tube) used to control gas flow had an accuracy of ±5%. The temperature was measured with industrial PT100 sensors with an accuracy of ±0.5°C.

2.2. Capacitance sensor

The capacitance sensor used in this research was developed in-house based on the AD7746 microchip, an integrated ΔΣ capacitance-to-digital converter from Analog Devices [17]. The converter can measure capacitances up to 21 pF with an accuracy of up to 4 fF ($4 \cdot 10^{-15}$ F), a resolution of 4 aF ($4 \cdot 10^{-18}$ F), and a frequency of up to 90 Hz, depending on the configuration. It operates based on a ΔΣ modulator with a maximum resolution of 24 bits and a square-wave excitation signal with a frequency of 32 kHz.

The measurement system was monitored by software running on a PC, see Fig. 2.

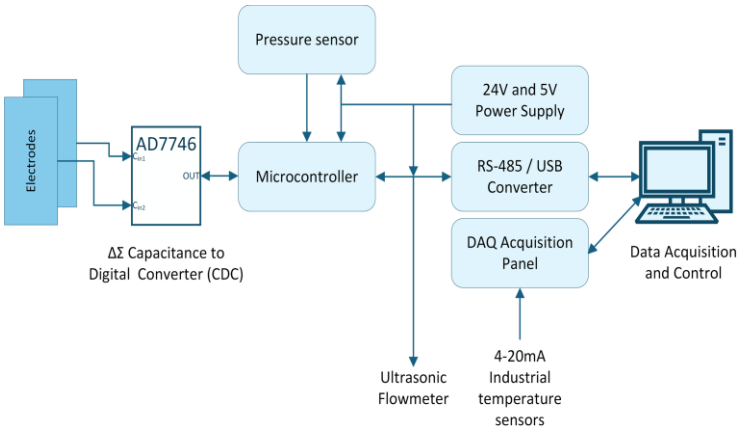

a)

b)

Fig. 2. Capacitance sensor with ΔΣ CDC: a) block diagram of the sensor components; b) photograph of the sensor board end electrodes mounted in the test section.

The RS-485 interface allowed for configuration and readout of the AD 7746, as well as readings from the ultrasonic flowmeter. Additionally, the DAQ panel connected to the Ethernet interface enabled readings from the temperature sensors. All read data was saved to a file every second.

2.3. Material properties

The relative permittivity of the materials used in the present study is listed in Table 1. The reservoir fluid came from the Lubiatów-Międzychód-Grotów (LMG) gas and oil field in western Poland. The air and methane were of industrial grade and were drawn from pressurised cylinders. The test section was made of a polycarbonate tube with inner and outer diameters of 45 mm and 50 mm.

Table 1. Relative permittivity.

Material	Relative permittivity ε_r (-)
Reservoir fluid	2.5
Air	1.00054
Methane	1.00081
Polycarbonate	2.9

The permittivity of the reservoir fluid was measured by the authors using the air capacitor method. It should be noted that it is only 2.5 times larger than that of the gases.

2.4. Test procedure

Measurements were performed at a constant flow rate and temperature. Capacitance values were sampled at a rate of 1 Hz. Each individual measurement for a specified flow parameter lasted 2 minutes, and the average capacitance during this time interval was recorded for further analysis. For each specified value of liquid flow rate, the liquid-only capacitance was first recorded. Next, two-phase flow capacitance measurements were taken for six values of injected gas flow rate. Before each series of measurements, the reservoir fluid temperature was stabilised at the desired level with an accuracy of ±2°C or better. Flash tank in the flow circuit ensured that the injected gas was removed and did not circulate in the test loop, its content did not increase during the two-minute data acquisition. Several photographs of the flow structure were also taken.

2.5. Supplementary numerical simulations

To gain insight into the phenomena occurring in the inter-electrode space of the capacitive sensor, numerical simulations were performed using the finite element method implemented in the FlexPDE 5 software [18,19]. The electrodes form a capacitor in which the distribution of the electric field in static conditions can be described by the Laplace equation [20]:

$$\nabla \cdot (-\varepsilon \nabla U) = 0, \tag{1}$$

where U denotes electric potential and $\varepsilon = \varepsilon_0 \varepsilon_r$ is absolute permittivity. Equation (1) was solved numerically in a cylindrical domain comprising a segment of the polycarbonate tube with two sensor electrodes, as shown in Fig. 3. The value of U at one of the electrodes was set to 0 and at the other to U_e = 0.625 V. The boundary condition on the outer surface of the solution domain was imposed in the form:

$$\nabla U \cdot \mathbf{n} = 0, \tag{2}$$

where **n** is a unit vector normal to this surface.

The condition (2) means that the electric field vector:

$$\mathbf{E} = -\nabla U, \tag{3}$$

is perpendicular to the outer surface of the domain, and the electrical charge induced on this surface is zero.

When the solution of Eq. (1) is known, the capacitance C can be calculated from the integral:

$$C = \frac{1}{V_e} \iint_S \varepsilon (\mathbf{E} \cdot \mathbf{n}) dS, \tag{4}$$

where S is a surface enclosing the excited electrode at the potential U_e, and $V_e = U_e$ is the voltage between electrodes.

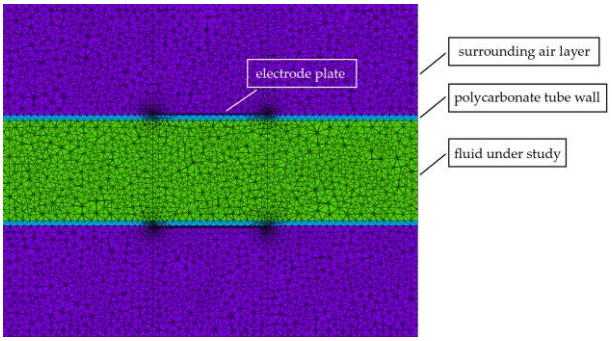

Fig. 3. Axial cross-section through the computational mesh (949 802 cells in total).

Details of the computational mesh are shown in Fig. 3. It forms a cylinder with a diameter of 150 mm and a length of 180 mm, which means that a 50 mm thick air layer was added around the outer walls of the polycarbonate tube and the electrode plates. The 50 mm wide plates were placed halfway along the tube. The mesh cells were generated automatically, but their size could be controlled. Mesh independence tests confirmed that meshes with approximately 1 million cells produced solutions with sufficient accuracy. Capacitance calculated for a fully filled tube with 1 million cells differs by around 0.1% from capacitance calculated with a minimum possible 300 thousand cells, and differs by around 0.01% from capacitance calculated with 2 million cells.

3. Results

The experiments began by assessing how the angular position and width of the electrode gap affected the capacitance readings. Next, with the electrodes set in their final configuration, tests were performed to evaluate the effect of liquid temperature. These measurements were done over a preselected range of fluid temperature, velocity and air void fraction. A similar set of experiments was later performed using methane instead of air. Finally, tests on the long-term stability and repeatability of the sensor concluded the study.

3.1. Effect of electrodes gap position and width

The performance of the capacitance sensor was investigated using three sets of electrodes with different gap widths: 3 mm, 26 mm and 40 mm, corresponding to 1/60, 1/6 and 1/4 of the pipe circumference, respectively. The width of each electrode was 50 mm. The effect of both gap size and angular position was investigated in the following sequence. First, the gaps were placed on the sides of the pipe, in the horizontal plane (0°). Next, the electrodes were rotated so that the centre of the gap was at a 45° angle. Finally, the gaps were placed at the top and bottom of the pipe, i.e. at a 90° angle. These gap positions and sizes are illustrated in Fig. 4.

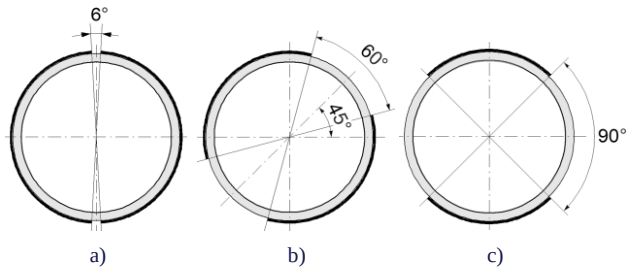

Fig. 4. Tested electrodes differing in gap angular position and width (note: each electrode size was tested at the three angular positions illustrated): a) large electrode at 90° angle (gap width 3 mm), b) medium electrode at 45° angle (gap width 26 mm), c) small electrode at 0° angle (gap width 40 mm)

Simultaneously with the measurement of electrical capacitance, photographs of the flow structure were taken on the pipe section upstream of the capacitance sensor.

During each test run, the flow rate was maintained at 5.8, 9.8, 13.9 or 17.8 m^3/h, corresponding to flow velocities in the test section ranging from 1 to 3.1 m/s. For each flow rate value, the air content in the reservoir fluid was increased stepwise from 0 to 4.2 L/min, which resulted in a maximum void fraction φ ranging from 1.4% in the fastest flow to 4.4% in the slowest one.

A single test series uses one electrode configuration and includes 28 individual measurements (4 liquid flow rates times 7 gas fraction values). For each test series, capacitance measured with only the reservoir fluid flowing (no gas added, void fraction equal to 0) served as the reference value, and was subtracted from the subsequent capacitances measured in two-phase gas-liquid flow. The resulting capacitance differences are shown in Figs. 5–7 for the three electrode sizes investigated, i.e. large, medium and small electrodes with the gaps of 3 mm, 26 mm and 40 mm, respectively. The fluid temperature during the tests ranged from 45°C to 55°C, with the variation of no more than ±2°C during a single measurement series.

The average capacitances measured for each electrode size and angular position are shown in Fig. 8 for liquid-only flow. The average value was calculated from 4 measurements corresponding to the number of flow rates tested. The standard deviation for these averages ranges from 0.001 pF to 0.004 pF, except for the large electrode at the 0° position, for which it is 0.008 pF.

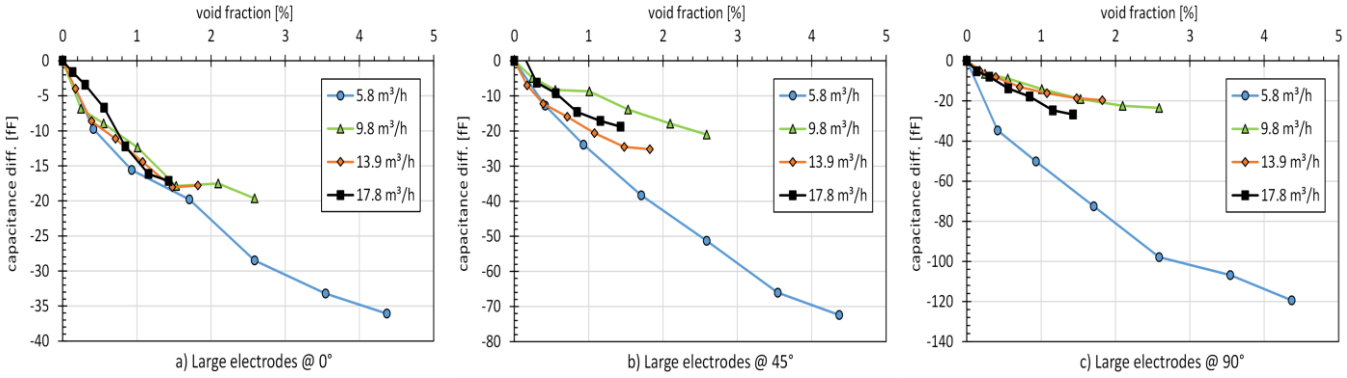

Fig. 5. Capacitance difference (in fF) measured for large electrodes (gap width 3 mm) in three gap angular positions.

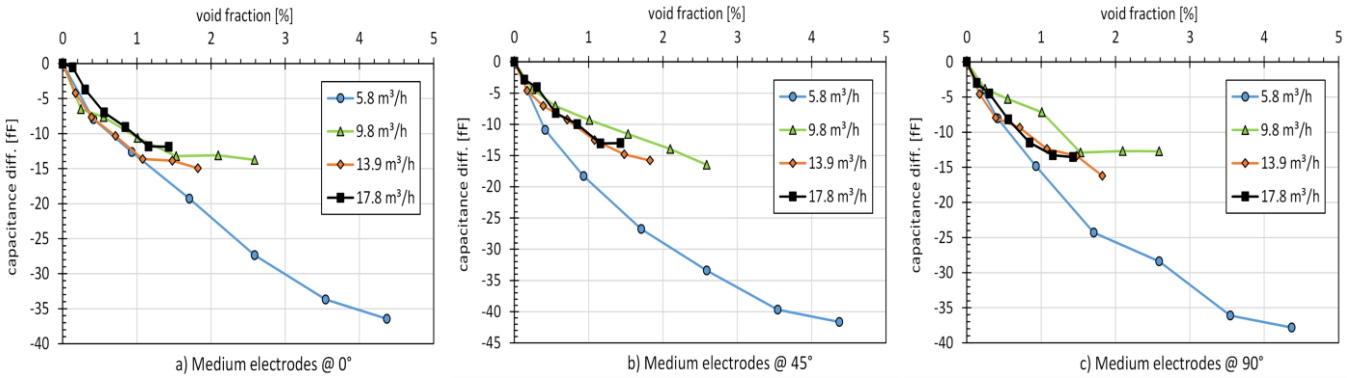

Fig. 6. Capacitance difference (in fF) measured for medium electrodes (gap width 26 mm) in three gap angular positions.

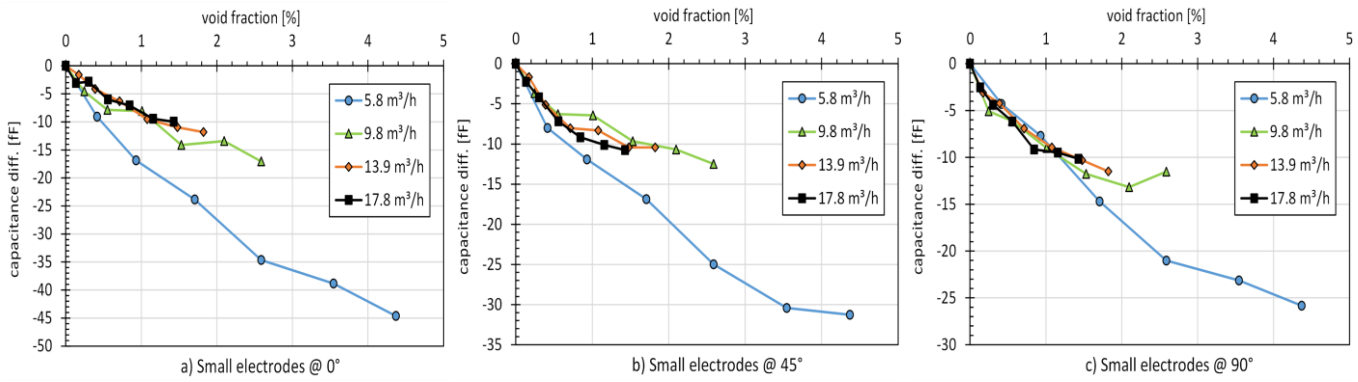

Fig. 7. Capacitance difference (in fF) measured for small electrodes (gap width 40 mm) in three gap angular positions.

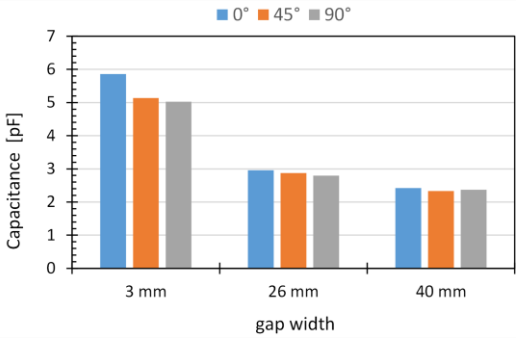

Fig. 8. Average capacitance measured for each configuration of the electrodes and liquid-only flow.

3.2. Effect of reservoir fluid temperature

The effect of fluid temperature on the capacitance sensor operation was checked using the largest electrodes with a 3 mm gap positioned at a 90° angle. For each measurement series, the temperature was constant and the set value was selected from 23°C to 50°C. For each temperature, the air content in the fluid was increased stepwise from 0 to 4.2%.

The test results for varying flow temperature are shown in Fig. 9, illustrating how the capacitance difference changes with air fraction. For each temperature tested, this relationship was measured sequentially for three liquid flow rates: 5.8, 9.8 and 13.9 m^3/h. As before, the capacitance difference was calculated using the value of liquid-only flow as a reference.

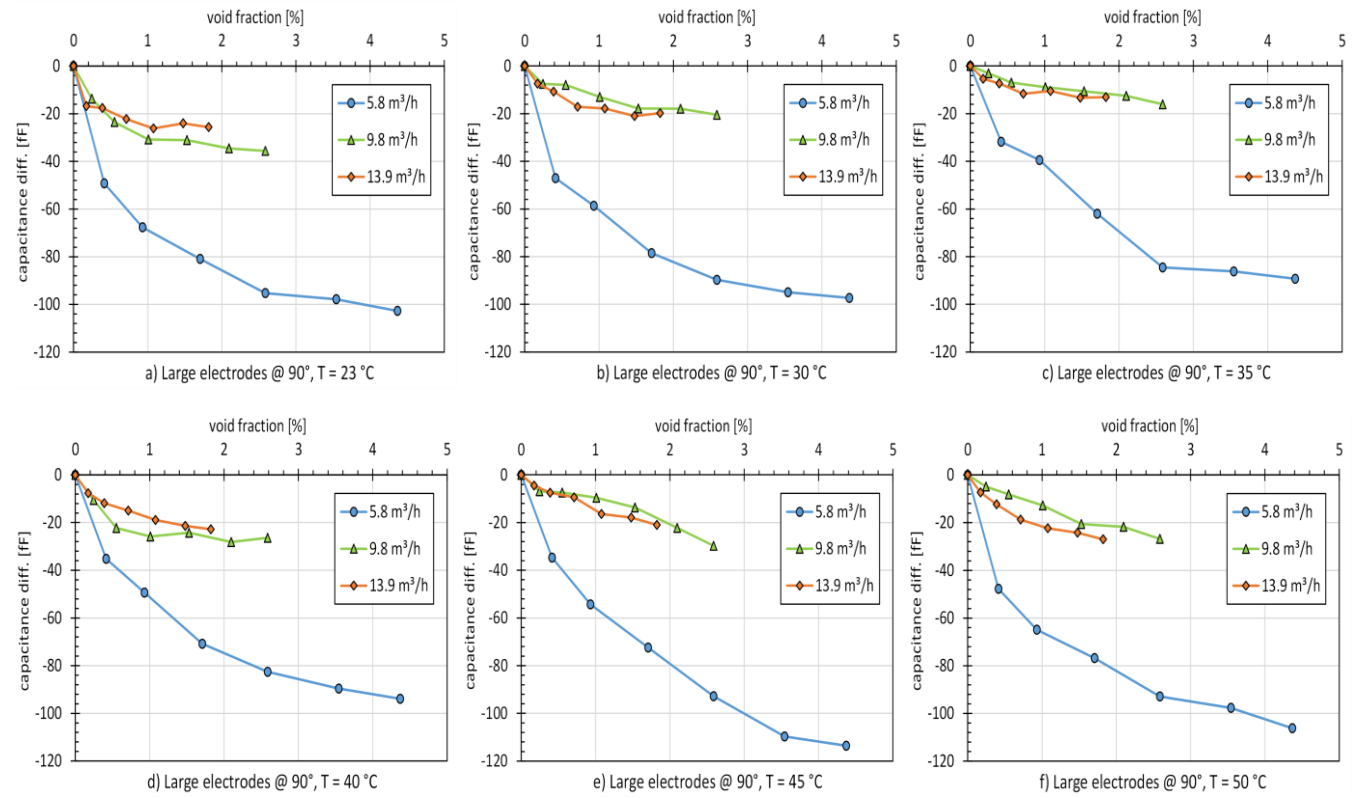

Fig. 9. Capacitance difference measured for large electrodes (gap width 3 mm at 90° angle) for selected reservoir fluid temperature values between 23°C and 50°C.

3.3. Test with methane

The tests with methane injection were carried out for fluid temperatures of 45°C and 50°C. Figure 10 shows the test results for methane. The format is the same as for the measurements with air injection. The capacitance difference relative to the value of liquid-only flow was calculated for three liquid flow rates of 5.8, 9.8, and 13.9 m^3/h. The volume flow rate of methane covers the same range as for the air case.

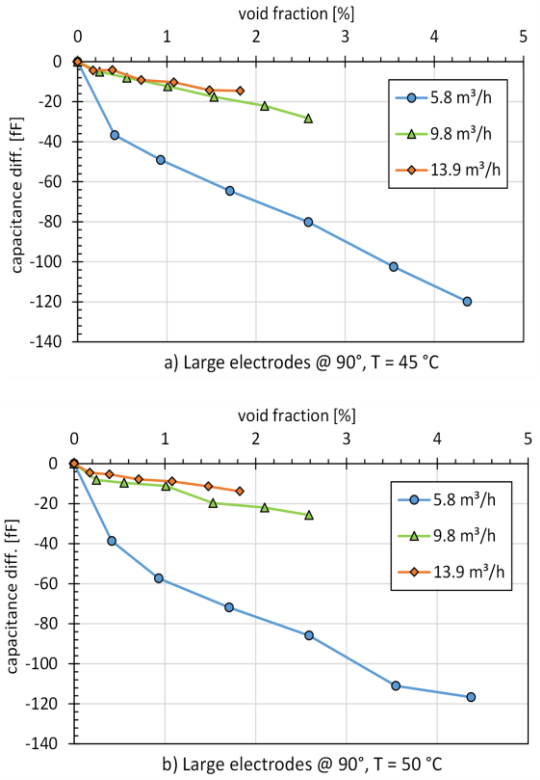

Fig. 10. Capacitance difference measured for large electrodes (gap width 3 mm at 90° angle) for methane injected into the reservoir fluid at temperature 45°C and 50°C.

3.4. Sensor repeatability tests

Continuous measurements of capacitance were taken under steady flow conditions to assess the stability of the sensor readings.

One of the stability tests examined the effect of reservoir fluid temperature on capacitance during a liquid-only flow, as shown in Fig. 11a. Continuous measurements were recorded for approximately 2 hours at 45°C. The temperature was then increased to 50°C, and recording continued for another 2 hours. The next day, the test at 50°C was repeated. All recorded capacitance values were within ±15 fF of the value recorded at the beginning of the measurement session on day one. Another stability test involved a gas injection period, as shown in Fig. 11b. The purpose of gas injection was to check whether the sensor readings returned to their initial level after the gas injection ended. It turned out that the capacitance in the second period of liquid-only flow was close to the initial level, although lower on average by about 4 fF.

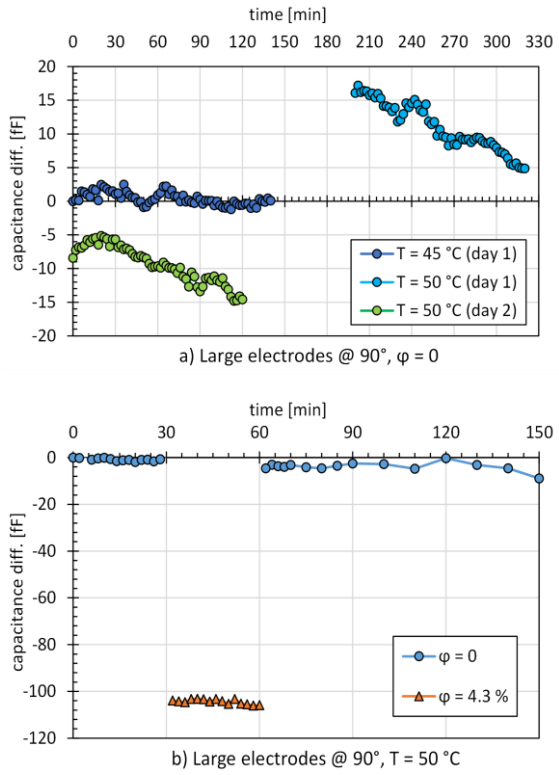

Fig. 11. Capacitance stability tests: a) repeatability of liquid-only capacitance, b) return of the sensor readings after a period of gas injection.

3.5. Flow structure photographs

Photographs of gas bubbles in the tube segment between the gas injection point and capacitance sensor were taken for each individual capacitance measurement. Figures 12 and 13 show example images that are typical for the used values of gas flow rate.

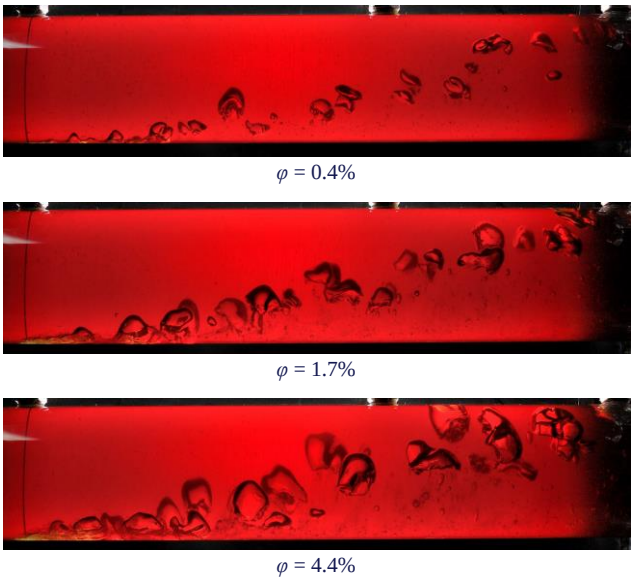

Fig. 12. Backlit photographs of flow patterns. Gas bubbles emerged from the needle outlet located at the bottom of the test tube, on the left. The capacitance sensor was located downstream (on the right), just outside the image. Liquid flow rate – 5.8 m^3/h, temperature – 52°C, void fraction φ = 0.4%, 1.7% or 4.4%.

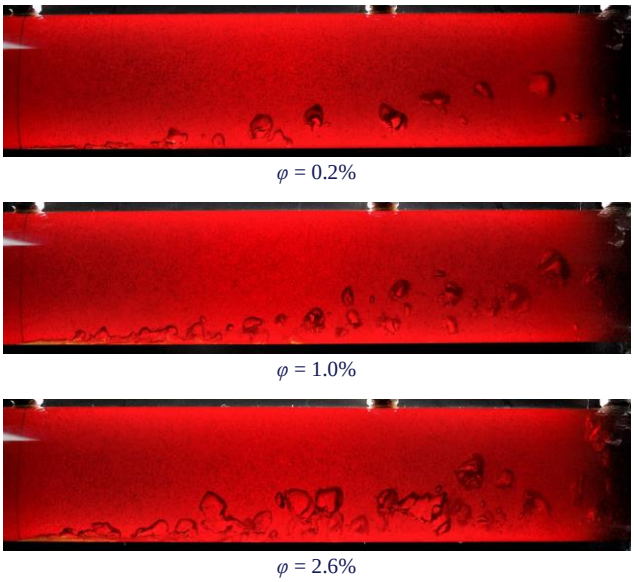

φ = 0.2%

φ = 1.0%

φ = 2.6%

Fig. 13. Backlit photographs of flow patterns. Gas bubbles emerged from the needle outlet located at the bottom of the test tube, on the left. The capacitance sensor was located downstream (on the right), just outside the image. Liquid flow rate – 9.8 m^3/h, temperature – 51°C, void fraction φ = 0.2%, 1.0% or 2.6%.

The photographs show the flow inside the polycarbonate tube viewed from the side, illuminated by light from the flash coming from behind the tube (backlight). Under this illumination, the colour of the reservoir fluid appeared red. The camera and flash were positioned in the horizontal plane. The gas was injected in the upstream part of the photographed segment, on the left in the images. The injection needle outlet was located near the bottom part of the tube inner wall, so the gas bubbles originate in the lower part of the images and move to the right, rising and expanding.

4. Discussion

The experiments discussed here aimed at reproducing reservoir fluid flow conditions similar to those found in a production well. Therefore, the temperature was elevated to 40–50°C in most tests. Due to limitations encountered (only one injection needle could be used), the maximum gas fraction in the flow did not exceed 4.4%. Nevertheless, the presence of gas was reliably detected by the capacitance sensor.

Most experiments have shown that capacitance differences due to increasing void fraction were greater at the lowest flow rate (5.8 m^3/h) than at higher rates. This difference decreased as the gap between the sensor electrodes increased, and was also more pronounced when the gaps were arranged vertically at the top and bottom of the test tube wall (position angle 90°, Fig. 4a). Similar trends appear in tests using methane instead of air.

Numerical simulations and photographs of actual flow explain the above-described effects. It turns out that the capacitance in the inter-electrode space depends not only on the amount of gas in the liquid, but also on its spatial distribution. As can be seen in Fig. 14, gas voids concentrating near the gap between the electrodes cause the largest decrease in capacitance.

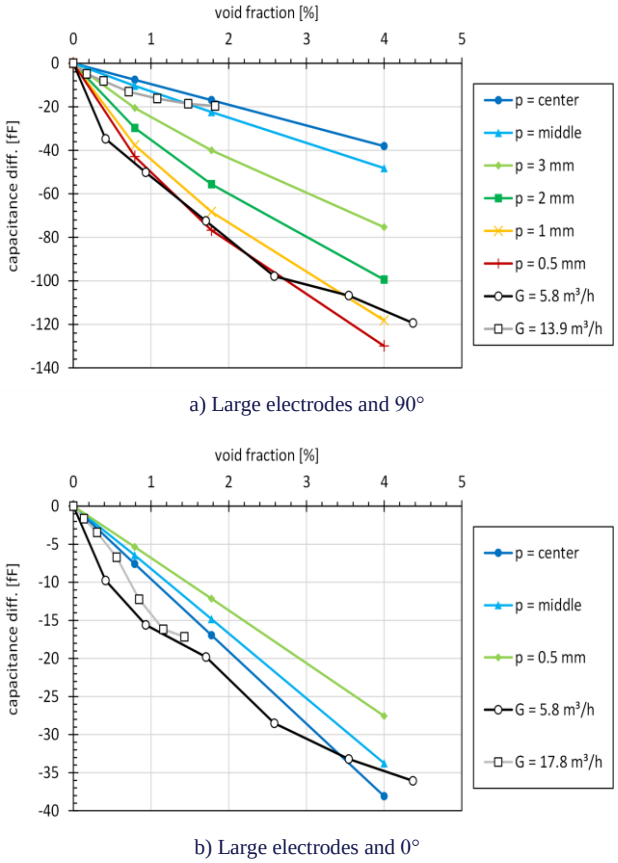

Fig. 14. Comparison of measurements with numerical simulations of capacitance changes depending on the void fraction and the void position "p" relative to the electrode plates. The effect of the void position is different when it approaches (a) the gap between the electrodes or (b) their centre.

The same amount of gas, when concentrated near the centre of the flow tube cross-section has a much smaller effect, as seen in Fig. 14a. The same can be said for gas concentration near the centre of the electrode plate, Fig. 14b. Comparison of the measurements with simulations leads to the hypothesis that for the lowest flow rate (and velocity), the injected gas created a bubble train that concentrated near the top of the tube wall, where the electrode gap at a 90° angular position was also located. For higher velocities and flow rates, the simulation results suggest that the gas bubbles concentrated and flowed along the centre of the tube. This is confirmed by the images of the flow patterns shown in Figs. 12 and 13. With this assumption about gas phase position in the tube cross-section, quantitative agreement is achieved between the measured and calculated capacitance difference values, Fig. 14a. Similarly, good agreement is also observed when the angular position of the gap was 0°, Fig. 14b. In this electrode configuration, bubbles flowing near the top of the tube cross-section approached the middle of the electrode plate and did not cause as large a capacitance drop as that near the gap. In summary, the concentration of gas voids in different areas of the tube cross-section causes different changes in electrical capacitance. Other researchers have reported this effect as well [7,8,21].

The calculated distributions of electric potential in the inter-electrode space, shown in Figs. 15 and 16, provide more details

on the influence of the location of gas voids. To explain these details, Figure 15 illustrates the potential distributions when the flow tube is completely filled with the reservoir fluid. The appearance of gas voids causes a disturbance of this potential, which affects the capacitance. Examples of potential distributions with voids representing gas bubble trains at a void fraction of 4% are shown in Fig. 16 (with the detailed views of parts of Figs. 16c and 16d presented in Fig. 17). The capacitance differences resulting from introduction of the voids can be found in Fig. 14 (position p = center, middle or 0.5 mm).

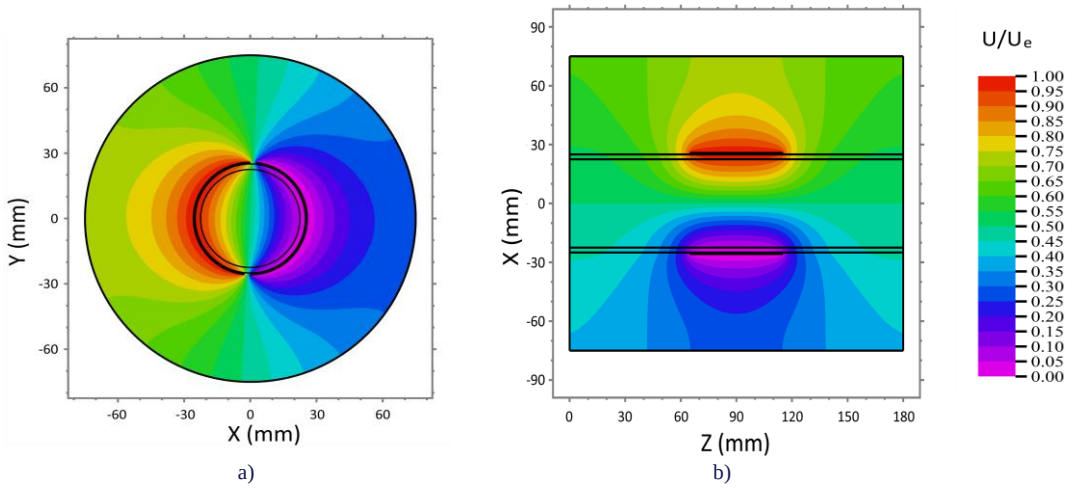

Fig. 15. Electric potential distributions in the inter-electrode space filled with reservoir fluid: a) transverse section in the middle of the electrodes, b) axial section.

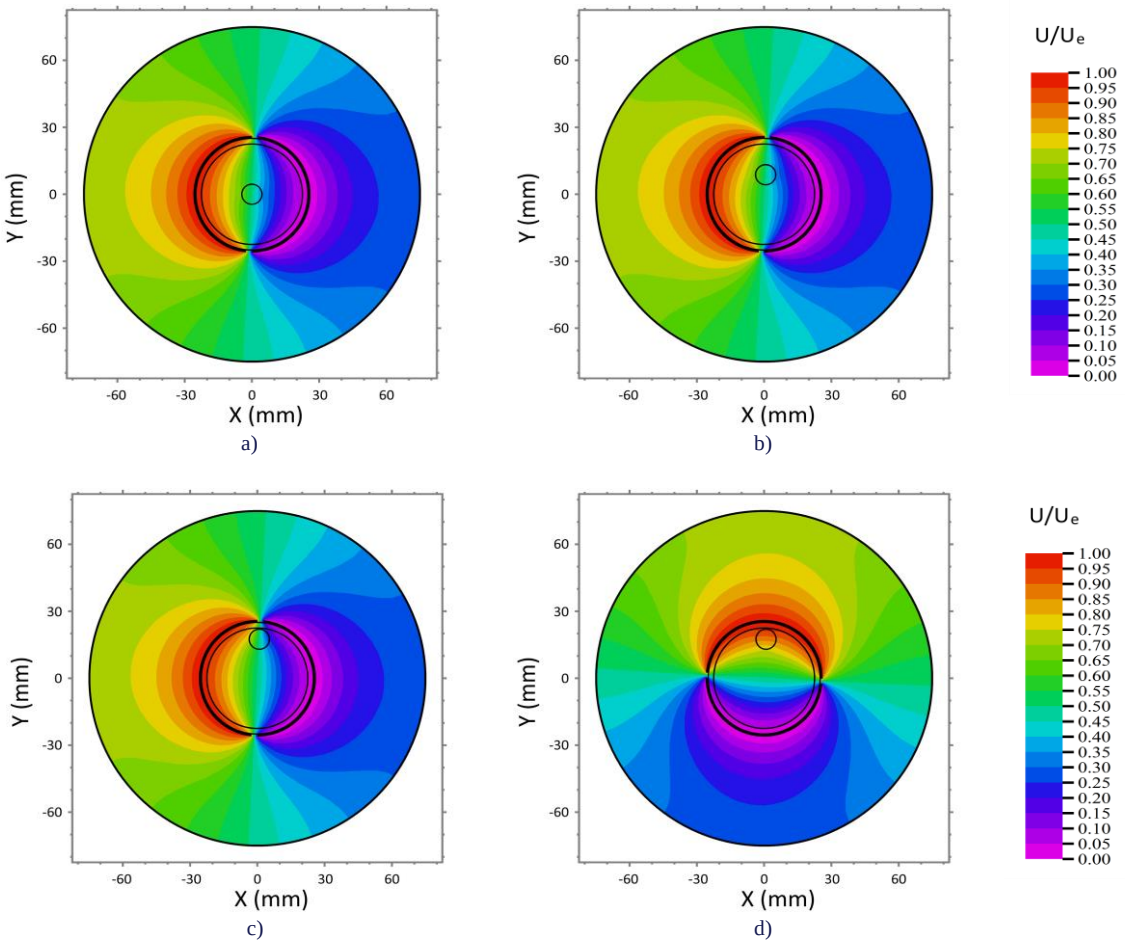

Fig. 16. Electric potential distributions in inter-electrode space for simulated two-phase flow with a 4% void fraction: a) gas phase concentrated in the tube centre, b) gas phase in the "middle" position shifted towards the gap, c) gas phase in the position 0.5 mm from the gap, d) gas phase in the position 0.5 mm from the plate centre.

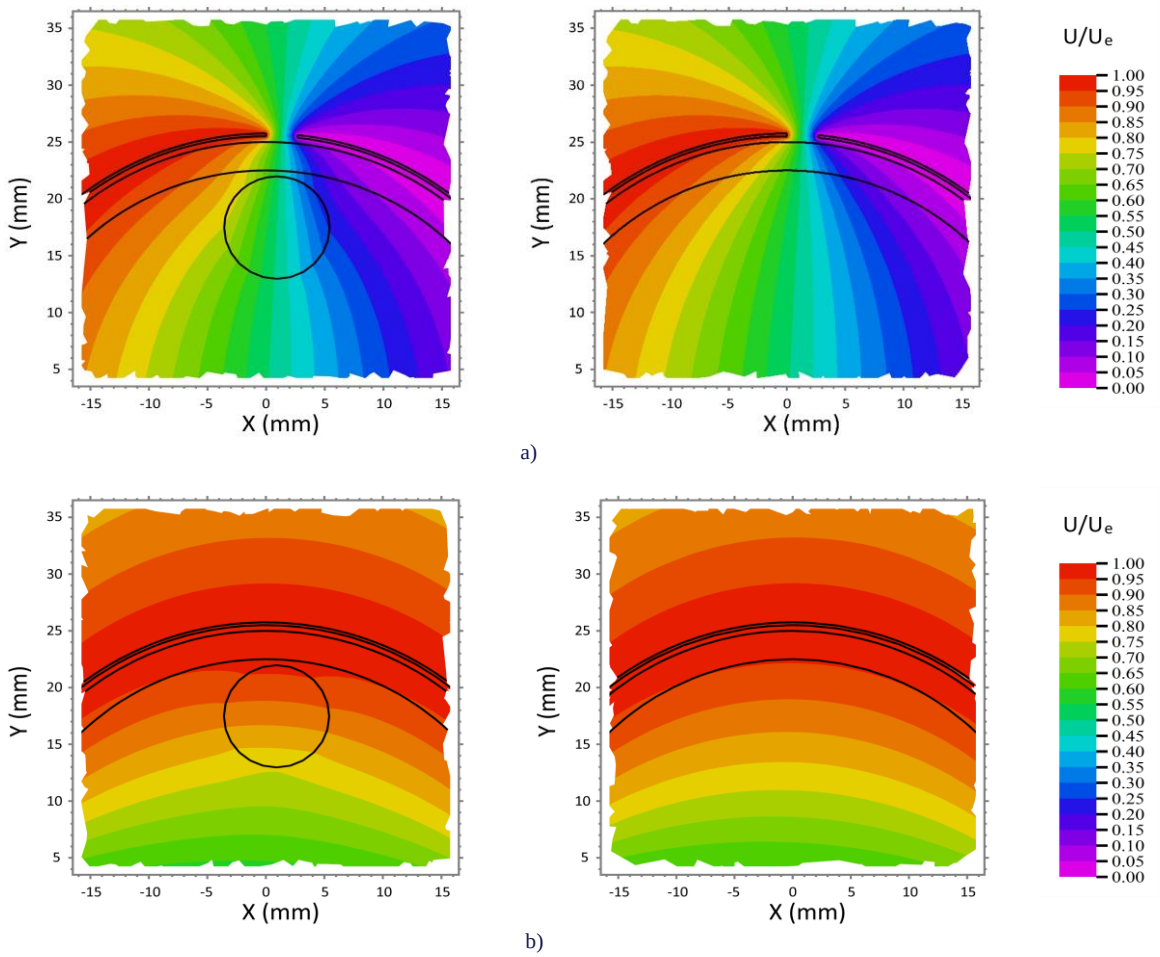

Fig. 17. Detail view of electric potential distributions near the simulated gas void with a 4% void fraction: a) gas phase in the position 0.5 mm from the gap, b) gas phase in the position 0.5 mm from the plate centre. Details at left are parts of Fig. 16c and 16d. Undisturbed liquid-only potentials are also shown at right for comparison.

The dependence of the measured capacitance difference on the electrode gaps angular position is weakest for large electrodes at 0° (when the gaps are located on the sides of the tube, Fig. 4c) or the gap itself is large, as in the tests with small electrodes (Fig. 7). However, as the gap increases (and therefore the plate becomes smaller), the measured capacitances decrease, as shown in Fig. 8. As a result, accurately measuring gas content becomes difficult due to the decrease in the signal-to-noise ratio. For example, the capacitance measured in liquid-only flow at temperatures of 45°C and 50°C averaged 5.23 ±0.05 pF, which is close to the value of 5.11 pF calculated from numerical simulations. The capacitance of gas-only flow, determined from the simulation, is 3.99 pF. Therefore, the full range of the sensor readings would be 1.12 pF.

The permittivity of the reservoir fluid varies with temperature [22], as verified in the tests described in Section 3.2. These measurements, however, did not demonstrate a clear relationship between capacitance and temperature. This is probably due to the fact that the change in the electrical capacity of the reservoir fluid in the tested temperature range from 23°C to 50°C was smaller than the measurement uncertainty of the sensor.

When methane instead of air filled the voids in the reservoir fluid, there were no significant changes in the measured capacitance difference. This conclusion can be supported by comparing the results in Fig. 5c or Fig. 9e,f and Fig. 10, where data for large electrodes with the gap at a 90° angle and flow temperatures of 45°C and 50°C are presented. In all these cases, the largest measured capacitance difference reached 120 fF for a flow rate of 5.8 m^3/h and a void fraction of 4.4%. At higher flow rates, this difference was much lower and amounted to approximately 30 fF at most.

For most liquid-only measurements, repeatability of 5 fF or better was achieved. Only for some tests of the reservoir fluid at 50°C, the repeatability was worse, reaching 15 fF. This means that the tested meter can measure with satisfactory accuracy the gas content above about 1% at low flow rates (corresponding to a velocity of about 1 m/s) and gas content above 2% at higher flow rates. Improving repeatability is only possible through periodic calibration of the device.

5. Conclusions

The experimental research described above concerned capacitance measurements of two-phase liquid-gas flow under conditions encountered during well testing and productivity monitoring in the oil and gas industry. Therefore, the liquid fraction used was actual reservoir fluid at elevated temperatures of 40–50°C.

To further increase the realism of the research, methane was intentionally used as the gas phase in some measurements to better simulate real-world conditions relevant to the study.

The following general conclusions can be drawn after analysing the experimental results discussed above:

- The commercial ΔΣ CDC can reliably detect small changes in capacitance, but quantitative measurements of small gas fractions require calibration of the sensor at the beginning of the measurement session.
- The measured capacitance value depends on both the gas fraction and the spatial distribution of voids in the reservoir fluid.
- Voids concentrated near the electrode gaps have the most significant impact on the capacitance drop in the inter-electrode space.

The capacitance sensor used in this research can be easily developed into a multi-electrode version that allows the reconstruction of the two-phase flow patterns.

Acknowledgements

This research was supported by the (Polish) National Centre for Research and Development (NCBR) under the Smart Growth Operational Program, grant number POIR.01.01.01-00-0780/15-00

References

[1] Kim, M., Komeda, K., Jeong, J., Oinuma, M., Sato, T., & Saito, K. (2022). Optimizing calibration for a capacitance-based void fraction sensor with asymmetric electrodes under horizontal flow in a smoothed circular macro-tube. *Sensors*, 22, 3511. doi: 10.3390/s22093511

[2] Qian, H., & Hrnjak, P. (2020). Mass measurement based calibration of a capacitive sensor to measure void fraction for R134a in smooth tubes. *International Journal of Refrigeration*, 110, 168−177. doi: 10.1016/j.ijrefrig.2019.10.019

[3] Hansen, L.S., Pedersen, S., & Durdevic, P. (2019). Multi-phase flow metering in offshore oil and gas transportation pipelines: trends and perspectives. *Sensors*, 19, 2184. doi: 10.3390/s19092184

[4] Okoro, E.E., Rachael, J.E., Sanni, S.E., & Emetere, M.E. (2021). Liquid holdup measurement in crude oil transportation using capacitance sensors and electrical capacitance tomography: concept review. *IOP Conference Series: Earth and Environmental Science*, 655, 012037, *4th International Conference on Science and Sustainable Development* (*ICSSD 2020*), *"Advances in Sciences and Technology for Sustainable Development"*, 3−5 August, Ota, Nigeria. doi: 10.1088/1755-1315/655/1/012037

[5] dos Santos, N.E., Reginaldo, N.S., Longo, J.N., da Fonseca Jr, R., Conte, M.G., Morales, R.E.M., & da Silva, M.J. (2024). Advancing oil and gas pipeline monitoring with fast phase fraction sensor. *Measurement Science and Technology*, 35, 125302. doi: 10.1088/1361-6501/ad73f5

[6] Salehi, S.M., Karimi, H., & Dastranj, A.K. (2017). A capacitance sensor for gas/oil two-phase flow measurement: exciting frequency analysis and static experiment. *IEEE Sensors Journal*, 17, 679–686. doi: 10.1109/JSEN.2016.2637399

[7] Salehi, S.M., Karimi, H., Moosavi, R., & Dastranj, A.K. (2017). Different configurations of capacitance sensor for gas/oil two phase flow measurement: An experimental and numerical study. *Experimental Thermal and Fluid Science*, 82, 349–358. doi: 10.1016/j.expthermflusci.2016.11.027

[8] Ahmed, W.H., & Ismail, B.I. (2008). Innovative techniques for two-phase flow measurements. *Recent Patents on Electrical Engineering*, 1, 1–13. doi: 10.2174/1874476110801010001

[9] Aslam, M.Z., & Tang, T.B. (2014). A high resolution capacitive sensing system for the measurement of water content in crude oil. *Sensors*, 14, 11351–11361. doi: 10.3390/s140711351

[10] Wolffenbuttel, R.F., & Regtien, P.P.L. (1987). Capacitance-to-phase angle conversion for the detection of extremely small capacities. *IEEE Transactions on Instrumentation and Measurement*, IM-36(4), 868–872. doi: 10.1109/TIM.1987.6312572

[11] Jaworek, A., & Krupa, A. (2010). Phase-shift detection for capacitance sensor measuring void fraction in two-phase flow. *Sensors and Actuators A*, 160, 78–86. doi: 10.1016/j.sna.2010.04.003

[12] Demori, M., Ferrari, V., Strazza, D., & Poesio P. (2010). A capacitive sensor system for the analysis of two-phase flows of oil and conductive water. *Sensors and Actuators* A, 163, 172–179. doi: 10.1016/j.sna.2010.08.018

[13] dos Reis, E., & da Silva Cunha, D. (2014). Experimental study on different configurations of capacitive sensors for measuring the volumetric concentration in two-phase flows. *Flow Measurement and Instrumentation*, 37, 127–134. doi: 10.1016/j.flowmeasinst.2014.04.001

[14] Abou-Arkoub, A., Thorn, R., & Bousbaine, A. (2010). Online validation of multiphase flowmeters using simple capacitance sensors. *IEEE Transactions on Instrumentation and Measurement*, 59(10), 2671–2682. doi: 10.1109/TIM.2010.2045554

[15] Wu, H., Tan, Ch., Dong, X., & Dong, F. (2015). Design of a Conductance and Capacitance Combination Sensor for water holdup measurement in oil–water two-phase flow, *Flow Measurement and Instrumentation*, 46, 218–229. doi: 10.1016/j.flowmeasinst.2015.06.026

[16] Maurya, O.P., & Parasuraman, S. (2024). Semi-cylindrical and cylindrical cross-capacitive sensors for micro-droplet detection. *Sensors and Actuators A*, 377, 115747. doi: 10.1016/j.sna.2024.115747

[17] *AD7746: 24-bit, 2 Channel Capacitance to Digital Converter*. Data sheet. https://www.analog.com/en/products/ad7746.html [accessed 23 July 2025].

[18] *FlexPDE – Multiphysics Software for Partial Differential Equations*. https://www.pdesolutions.com [accessed on 23 July 2025].

[19] Backstorm, G. (2004). *Fields of Physics by Finite Element Analysis: Electricity, Magnetism, and Heat in 2D and 3D. Using FlexPDE® Version 5*. GB Publishing, Malmö, Sweden.

[20] Guru, B., & Hiziroğlu, H.R. (2004). *Electromagnetic Field Theory Fundamentals* (2nd ed.). Cambridge University Press, Cambridge, UK.

[21] Tollefsen, J, & Hammer, E.A. (1998). Capacitance sensor design for reducing errors in phase concentration measurements. *Flow Measurement and Instrumentation*, 9, 25–32. doi: 10.1016/S0955-5986(98)00006-5

[22] Alvarez, J.O., Jacobi, D., Althaus, S., & Elias, S. (2012). Dielectric characterization of geochemical properties of liquid hydrocarbons 25°C to 125°C. *Fuel*, 288, 119679. doi: 10.1016/j.fuel.2020.119679